HHS Public Access

Author manuscript

J Tissue Eng Regen Med. Author manuscript; available in PMC 2020 November 01.

Published in final edited form as:

J Tissue Eng Regen Med. 2019 November ; 13(11): 1965–1977. doi:10.1002/term.2946.

Promotion of Dermal Regeneration using Pullulan/Gelatin Porous Skin Substitute

Nan Cheng[1], **Marc G Jeschke**[*,1,2,3,4,5], **Mohammadali Sheikholeslam**[1], **Andrea-Kaye Datu**[1], **Hwan Hee Oh**[1], **Saeid Amini-Nik**[*,1,3,6]

[1]Sunnybrook Research Institute, University of Toronto, Toronto, ON M4N 3M5, Canada

[2]Institute of Medical Science, University of Toronto, Toronto, ON M5S 1A8, Canada

[3]Department of Surgery, University of Toronto, Toronto, ON M5T 1P5, Canada

[4]Department of Immunology, University of Toronto, Toronto, ON M5S 1A8, Canada

[5]Ross-Tilley Burn Centre, Sunnybrook Health Sciences Centre, Toronto, ON M4N 3M5, Canada

[6]Department of Laboratory Medicine and Pathobiology, University of Toronto, Toronto, ON M5S 1A8, Canada

Abstract

Tissue engineered dermal substitutes represent a promising approach to improve wound healing and provide more sufficient regeneration, compared to currently clinical standard of care of large wounds, early excision and grafting of autografts. However, inadequate regenerative capacity, impaired regeneration/degradation profile and high cost of current commercial tissue engineered dermal regeneration templates hinder their utilization and the development of an efficient and cost-effective tissue engineered dermal substitute remains a challenge. Inspired from our previously reported data on pullulan/gelatin scaffold, here we present a new generation of a porous pullulan/gelatin scaffold (PG2) served as a dermal substitute with enhanced chemical and structural characteristics. PG2 shows excellent biocompatibility (viability, migration, and proliferation), assessed by *in vitro* incorporation of human dermal fibroblasts (HDFs) in compare with the Integra® dermal regeneration template (Control). When applied on a mouse full-thickness excisional wound, PG2 shows rapid scaffold degradation, more granulation tissue, more collagen deposition and more cellularity in comparison with Control at 20 days post-surgery. The faster degradation is likely due to the enhanced recruitment of inflammatory macrophages to the scaffold from the wound bed and that leads to earlier maturation of granulation tissue with less myofibroblastic cells. Collectively, our data reveal PG2's characteristics of an applicable dermal substitute with excellent dermal regeneration which may attenuate scar formation.

[*]Corresponding authors: Saeid Amini Nik : saeid.amininik@utoronto.ca, Marc G Jeschke: marc.jeschke@sunnybrook.ca.

Supporting Information

Supporting Information is available from the Wiley Online Library or from the author.

Conflicts of interest

The authors declare that there is no competing financial interest.

Keywords

pullulan; gelatin; scaffold; dermal substitute; skin regeneration; wound healing

1. Introduction

Skin plays a crucial role in protection from external threats, provides sensation and contributes in fluid homeostasis. Insults to the skin such as deep cuts, burns or ulcers could cause damage to the skin and further compromise the clinical outcome. In conditions like burn which the skin loss is extensive, grafting from different sources is inevitable. In these occasions, conventional treatments for skin damage include autografts, allografts, and xenografts, which have been extensively used surgically. However, due to the limitation of donor sites or the high risk of immunological rejection grafting has its own limitations (Rnjak, Wise, Mithieux, & Weiss, 2010; B. K. Sun, Siprashvili, & Khavari, 2014). With rapid development of regenerative medicine, engineered skin substitutes have become a promising alternative treatment to promote dermal tissue regeneration. The proper skin substitutes are required to provide architectural support and microenvironment for cell infiltration and growth. Some of these currently studied skin substitutes have been proven in improving long-term skin function and appearance (Branski et al., 2007; N. Moiemen et al., 2011; N. S. Moiemen, Staiano, Ojeh, Thway, & Frame, 2001; Soller, Tzeranis, Miu, So, & Yannas, 2012). However, autografts are still the gold standard for treating skin loss if sufficient donor site is available mainly due to the lack of optimal engineered scaffolds to substitute dermal tissues.

Among various materials studied for dermal regeneration, combinations of gelatin with polysaccharides are one of the highly recognized choices (Aljghami, Saboor, & Amini-Nik, 2019; Sheikholeslam, Wright, Jeschke, & Amini-Nik, 2017). This combination has been used to not only maintain the mechanical strength of biomaterials but also enhance cell survival and proliferation. Gelatin is among the most popular natural proteins to construct scaffolds in tissue engineering and has been extensively studied and commercially utilized in skin substitutes due to its good biocompatibility and excellent support on cell growth (H.-M. Wang et al., 2013; T.-W. Wang et al., 2006; Xiong et al., 2017; Zhao et al., 2016; Zhao et al., 2017). Amongst polysaccharides studied for skin regeneration, pullulan is a fungal polysaccharide consisting of three glucose units connected by α−1,4 glycosidic bonds (maltotriose) and consecutive maltotriose units connected by α−1,6 glycosidic bonds (Leathers, 2003). It has attracted attention because of its anti-inflammatory, anti-bacterial, and anti-oxidant properties, as well as its lack of immunogenicity and its low cost (X. Li et al., 2015; Mano et al., 2007; Mathew N. Nicholas, Marc G. Jeschke, & Saeid Amini-Nik, 2016; Rustad et al., 2012; Wong et al., 2011).

We recently reported a pullulan/gelatin scaffold with a high pullulan composition to deliver progenitor fibroblasts and keratinocytes (Mathew N Nicholas, Marc G Jeschke, & Saeid Amini-Nik, 2016). While promising, its instability during transportation and handling particularly when we scaled it up in size, and its improvable biocompatibility in order to provide satisficed cell migration and growth environment are factors hindering its

application in the clinic. Thus, the purpose of this study was to develop a cell supporting pullulan/gelatin (PG) scaffold with enhanced biocompatibility and increased crosslinking that would allow for easy handling of the large scaffold. By optimizing the P/G ratio and introducing dual-crosslinking, here we report the second generation of the PG scaffold (PG2) and investigate its material properties, biocompatibility, and therapeutic potential as a dermal skin substitute.

2. Materials and Methods

2.1 Preparation of PG2 scaffolds

PG2 was prepared through a combined salt-leaching/crosslinking method. First, 1 g of sodium chloride (NaCl) was added into a 3.5 cm petri dish as the porogen, followed by the mixture of 100 μL 0.2 g mL^{-1} pullulan (Sigma-Aldrich, Oakville, ON, Canada) aqueous solution and 200 μL 0.1 g mL^{-1} gelatin (Type A, BioShop, Burlington, ON, Canada) aqueous solution, and an extensive mixing action. Second, 10 mg trisodium trimetaphosphate (STMP) (Sigma-Aldrich) with 5 μL 10N sodium hydroxide solution (NaOH) was mixed in 200 μL water and then added into the petri dish, followed by an extensive mixing action. The final mixture in the petri dish was then put into an oven at 60 °C for 3 h. The solidified resultant was washed by PBS at 4 °C until pH on the material was maintained at pH 7. In order to crosslink gelatin, 200 mM 1-ethyl-3-(3-dimethylaminopropyl)carbodiimide hydrochloride / 80 mM N-hydroxysuccinimide (EDC/NHS, Thermo Fisher Scientific, Waltham, MA, USA) aqueous solution was prepared right before use, and 2 mL of EDC/NHS solution was added onto the solidified material for crosslinking. The reaction was conducted at 4 °C overnight, and the reactant was washed with PBS for 12 h by changing the medium every 2 h. The final product was freeze-dried and stored at 4 °C before use.

2.2 Material characterization

Morphology of PG2 was examined by scanning electron microscope (XL30 ESEM, FEI, Hillsboro, OR, USA) operating at 20 kV. Dry PG2 scaffolds (8 mm in diameter biopsies) from lyophilization were used to observe its hydrated morphology. A coating of 20 nm Au by the sputter coater (Leica ACE600, Concord, Ontario, Canada) was applied onto samples before the examination. μCT (Scanco Medical μCT100, Brüttisellen, Switzerland) was used on dry PG2 (8 mm biopsies) to generate description and visualization of the 3D porous structure. The achieved resolution of 8 mm biopsied PG2 sample was 3 μm per voxel in each axis.

Swelling of PG2 scaffolds (8 mm biopsies) was evaluated in water at 37 °C. Size changes in diameter were measured manually at different time points until the equilibrium state was reached by about six hours. The swelling behavior was profiled by diameter change vs. time. Water retention capacity of PG2 was calculated by mass of the hydrated 8 mm biopsied PG2 at its equilibrium state vs. the lyophilized 8 mm biopsied PG2.

To assess biodegradation, PG2 scaffolds (8 mm biopsies) were placed into a 60 μg mL^{-1} (7.5 unit mL^{-1}) collagenase I (Thermo Fisher Scientific) PBS solution, pH = 7.4, and incubated

at 37 °C with 5% CO_2 and 100% humidity (Lee, Kim, Chong, Hong, & Lee, 2005). After the determined time, the scaffolds were removed from the enzyme solution, washed with deionized water for three times, and weighted after lyophilization. The remaining weight (%) was calculated using the following equation (1):

$$\text{remaining weight} = W_t/W_0 \times 100, \quad (1)$$

where W_0 is the initial weight of the dry scaffold and W_t is the weight of the dry scaffold after degradation at the time of t.

2.3 Human skin tissue sampling and cell culture

The normal human skin tissues were obtained from healthy donors (undergoing reconstructive surgery procedures) at Ross Tilley Burn Centre, Sunnybrook Health Sciences Centre, Toronto, ON, Canada. Collection of skin tissue samples has followed the approval of the Institutional Ethics Review Board (Declaration of Helsinki Principles, Academic Health Sciences Network and University of Toronto-affiliated Sunnybrook Research Institute and Sunnybrook Health Sciences Centre). Informed signed consent was obtained from the patients (REB PIN 142–2015 and UHN REB# 13–6437-CE). Normal human skin dermis was used to obtain normal human fibroblasts through primary cell culture technique (Arno, Amini-Nik, Blit, Al-Shehab, Belo, Herer, Tien, et al., 2014; Bakhtyar, Jeschke, Mainville, Herer, & Amini-Nik, 2017). The study has been approved and reviewed by the REB/IRB of Sunnybrook Research Institute.

Human primary dermal fibroblasts (HDFs) were obtained from normal human skin tissue samples. Normal skin tissue specimen were cleaned to remove fat and cut into small pieces (sized of 2 to 4 mm) known as the explants. Explants were cultured in small Petri plates (37 °C in a humidified atmosphere with 5% CO_2) to obtain primary fibroblast cells. Primary fibroblasts were sub-cultured in Petri plates (density of 3,200 cells cm^{-2}) for one week and later subjected to next passaging. The primary culture (70% confluency) was subjected to trypsinization (0.05% trypsin) and further sub-cultured (4,500 cells cm^{-2}) in flasks (Corning® cell culture flasks, 75 cm^2).

2.4 *In vitro* cell incorporation

HDFs were cultured in high-glucose Dulbecco's modified Eagle's medium (DMEM) supplemented with 10% (v/v) FBS (Gibco, Thermo Fisher Scientific) and 1% (v/v) antibiotic-antimycotic solution, and incubated at 37 °C in a 5% CO_2 atmosphere incubator. Media was changed every 48 h. For sterilization of the scaffolds, 8 mm biopsies of PG2 and the Integra® dermal regeneration template (Integra Life Sciences, Plainsboro, NJ, USA, abbreviated as Control hereafter) were placed in a 48-well plate and sterilized by ultra violet light for 30 min. The UV sterilization was performed inside a biosafety cabinet equipped with a germicidal UV lamp of 255–280 nm. The distance between the UV lamp and the object was the distance between the lamp and the floor of the cabinet (100 cm). Sterile PBS solution was added into the plate to pre-dissolve the scaffolds 24 h before seeding. Prior to seeding, fibroblasts within a passage of 10 were trypsinized and re-suspended in the medium at a concentration of 2×10^5 per mL. A cell suspension (10 μL) was added onto scaffolds

placed in a 48-well plate. Facilitate the cell uptake into the interior of the scaffold for 1 h in the incubator and then add 500 μL medium to each well. The medium was changed every 48 h.

2.5 Cell Viability and Cell Proliferation

Cell viability was determined by a Live/Dead Viability/Cytotoxicity Kit (Life Technologies, Calsbad, CA, USA) on HDF-incorporated scaffolds at day 3, 7 and 14 post seeding respectively. 3D images of cell migration at day 3, 7 and 14 were taken through Z-stack function of Zeiss observer Z1 spinning disc confocal microscope. Cell proliferation at day 7 was determined by 5-bromo-2'-deoxyuridine (BrdU) proliferation assay. The HDF-incorporated scaffolds were incubated with 10 mM BrdU (EMD Chemicals, San Diego, CA, USA) in the medium for 24 h. The medium was removed, and the samples were washed with PBS. A Thermo Fisher Scientific BrdU Labeling and Detection Protocol was followed. BrdU (Bu20a) Mouse monoclonal antibody from Cell Signaling Technology (Danvers, MA, USA) and Alexa Fluor® 488–labeled Donkey anti-Mouse IgG (H + L) secondary antibody from Invitrogen (Carlsbad, CA, USA) were used in the protocol. 4',6-Diamidino-2-phenylindole dihydrochloride (DAPI) was applied at the last step to visualize all cells. Quantification of the percentage of BrdU positive cells was performed by counting the number of BrdU-positive cells vs. the total number of cells. In transforming growth factor-beta1 (TGF-β1) inducing study, the medium was changed to serum-free DMEM 48 h after seeding 1×10^4 HDFs on PG2 and Control. After 24 h, TGF-β1 (15 ng/mL, PeproTech, Montreal, QC, Canada) in serum-free DMEM was added to treat the cell-incorporated PG2 and Control. Immunofluorescence staining was preformed after 48 h. Briefly, cells in the scaffolds were fixed with 4% paraformaldehyde in PBS for 20 min at room temperature. Fixed cells were washed with PBS three times followed by permeabilization with PBST solution (PBS/0.25% Triton X-100 (Sigma-Aldrich) solution) for 10 min. After washing and blocking with 1% bovine serum albumin (BSA; BioShop) in PBST solution, the samples were incubated with anti-α-smooth muscle actin (anti-ASM) primary antibody (α-smooth muscle actin (1A4) mouse monoclonal antibody from Cell Signaling Technology) for 1 h at room temperature. After three washings with PBS, samples were then treated with the secondary antibody, goat anti-mouse IgG (H+L) $F(ab')_2$ Fragment (Alexa Fluor® 647 conjugate) (Cell Signaling Technology). Finally, the samples were counterstained with DAPI.

2.6 *In vivo* mouse study

8-week-old Male C57BL/6 mice (Jackson Laboratories, Bar Harbor, ME, USA) were used for excisional wound model experiments (n = 10). The study was under the guidelines of the Sunnybrook Research Institute and Sunnybrook Health Sciences Animal Policy and Welfare Committee of the University of Toronto. Animal procedures were reviewed and approved by Sunnybrook Research Institute and Sunnybrook Health Sciences Centre at University of Toronto Animal Care and Use Committee. Animals were anesthetised, and two 6 mm-diameter full-thickness wounds were created on the back of the mouse on either side from the midline (M. G. Jeschke, A.-R. Sadri, C. Belo, & S. Amini-Nik, 2017). The wound treatments were randomly divided into two groups: PG2 and Control. Each wound used a customer-designed twist-open plastic dome to prevent skin contraction and mimic wound

healing in human skin. The dome on the mouse was to allow the skin to stretch and secure the applied skin substitutes. An 8 mm skin substitute (either PG2 or Control) was placed inside the dome(Aljghami, Jeschke, & Amini-Nik, 2019; M. G. Jeschke, A. R. Sadri, C. Belo, & S. Amini-Nik, 2017). The wounds were monitored daily until 20 days post the surgery to determine the general conditions of the wounds and the treatments. Pictures were not taken in order to prevent further damage to the wound healing process. The mice were then euthanized, and the excised wounds were collected for histologic analysis.

2.7 Masson's trichrome staining

All reagents for Masson's trichrome staining were purchased from Electron Microscopy Sciences (EMS; Hatfield, PA, USA) unless otherwise mentioned. Harvested tissues were embedded in paraffin, cut at 5 μm thickness and mounted on Superfrost™ Plus glass slides (Fisher Scientific, Pittsburgh, PA, USA). The procedure was conducted as follows: slides were heated at 60 °C for 30 min, deparaffinized with Citrosol (Decon Laboratories, King of Prussia, PA, USA) and rehydrate through 100%, 95%, and 70% ethyl alcohol. After washed with distilled water, the slides were further fixed in Bouin's solution overnight at room temperature. Then the slides were washed again under a running tap water to remove the yellow color, and dipped into Weigert's iron hematoxylin working solution for 10 min. After, they were washed under distilled water, stained in Biebrich scarlet-acid fuchsin for 10 min, and washed again with distilled water. Next, the slides were differentiated in phosphomolybdic-phosphotungstic acid solution for 15 min and transferred directly into the aniline blue solution for 5 min. Finally, the slides were rinsed briefly in distilled water, differentiated in 1% acetic acid solution for 2 min, and washed in distilled water. At last the slides were dehydrated quickly using 95% and 100% alcohol and cleared in Citrosol. The stained slides were mounted with a coverslip by xylene-based mount medium (General Data Company, Cincinnati, OH, USA).

2.8 Immunohistochemistry and immunofluorescence

Paraffin-embedded tissues sections were studied by either immunohistochemistry or immunofluorescence analysis of CD31 for microvessels, F4/80 for macrophages and ASM for myofibroblasts. For immunohistochemistry, sections were first deparaffinized as described above. Then, a heat-based antigen retrieval step was performed, followed by 3% H_2O_2 incubation to inactivate the endogenous peroxidase. The tissues were then treated with the specific primary antibody (purified NA/LE rat anti-mouse CD31 Clone 390 from BD Biosciences, San Jose, CA, USA; anti-F4/80 polyclonal antibody from Abcam, Cambridge, UK) at the recommended dilution. A species-appropriate MACH3 horseradish peroxidase (HRP)-polymer detection kit followed by a betazoid diaminobenzidine chromogen kit (Biocare Medical, Concord, CA, USA) was applied to generate a brown color. Slides were then counterstained with hematoxylin, differentiated in 1.5% acid alcohol and then placed in 0.1% sodium bicarbonate very briefly. Finally, the slides were mounted with a coverslip using xylene-based mounting medium after dehydration. For immunofluorescence staining, a proteinase-K method was performed for antigen retrieval after deparaffinization, followed by cell permeabilization with PBST solution. After blocking the sections with 1% BSA in PBST solution, they were treated with the anti-ASM primary antibody for overnight. The biotinylated secondary antibodies (Vector Laboratories, Burlington, ON, Canada) were then

added in PBST solution with 1% BSA for 1 h at room temperature, followed by fluorescent streptavidin probe (549 nm, Vector Laboratories) for 20 min. Finally, the slides were mounted with Vectashield mounting medium with DAPI (Vector Laboratories).

2.9 Imaging and quantification

Trichrome and immunohistochemistry stained sections were observed using a Zeiss Axiovert 200 light microscope at 40X magnification, e.g., high power field (HPF). Immunofluorescence images were taken through a Zeiss observer Z1 spinning disc confocal microscope. The size of granulation tissues was quantified according to trichrome stained whole wound sections. Quantification of collagen deposition was performed on trichrome stained HPF images. Quantification of infiltrated cell number was performed on five DAPI stained HPF images from the center of the scaffold areas in the wound sections for each group. Quantification of angiogenesis was performed by counting the number and the size of vessels per HPF. Proportions of F4/80 positive cells either from the scaffolds or from the wound beds were calculated respectively based on five representatives images in each group. Proportions of ASM positive cells from the center of the scaffold areas of the histological sections or from *in vitro* HDF seeded scaffolds were determined from nine representative images each group. Quantification was performed blindly and with the assistant of ImageJ software. Data are presented as mean ± SEM.

2.10 Statistical Analysis

Statistical analysis was performed using Two-Sample *t*-Test. $P < 0.05$ was considered statistically significant. The error bars represent SEM.

3. Results

3.1. Preparation and properties of PG2

As depicted in Figure 1A, the 3D porous PG2 was developed using a particulate leaching method combined with crosslinking. The mixture of pullulan and gelatin was blended with salt particulates as porogens. Pullulan was crosslinked by a non-toxic and FDA-approved reagent STMP. Gelatin was crosslinked between carboxylic acid and primary amine functional groups with the zero-length carbodiimide EDC accompanied by NHS.

To acquire the structural characteristic of PG2, scanning electron microscope (SEM) and *X-ray* micro-tomography (μCT) techniques were applied to obtain the 2D and the 3D microstructure of PG2. As the SEM images were shown in Figure 1B, a highly porous structure was developed within PG2. Heterogeneous round-shaped pores were observed and the interconnectivity of its porous structure was shown in the cross-sectional image of PG2. The pore sizes ranged from 20 – 198 μm. The porosity of PG2 was calculated as 73.54 ± 3.24% based on the area fraction of void area vs. total area from the SEM images. Additional to SEM, a comprehensive 3D overview of the morphological and the architecture of PG2 was provided in Figure S1 by μCT.

Water retention and the swelling behavior of PG2 were studied by gravimetry. PG2 can retain 797.7 ± 56.9% of water of its dry mass at equilibrium hydrated state. A fast swelling

profile was observed (Figure 2A). Dry PG2 swelled and adopted its equilibrated size within a short period of time (20 min) upon contact with water. However, the equilibrium hydration state of the scaffold could take a longer period of time as depicted in Figure 2A. The response of PG2 to collagenase digestion was profiled to determine its biodegradability. Mass loss of PG2 was recorded via immersion of the scaffold into collagenase I solution over a 5-day period (Figure 2B). A relatively fast degradation was observed at the first 24 h, showing a 66% reduction of PG2. Passing that early fast degradation phase of 24 hours, 26% of the PG2 stayed at 5 days.

3.2. Biocompatibility of PG2

Cell viability was investigated at different time intervals post seeding in order to determine biocompatibility of PG2 in term of cell adhesion, cell growth, and cell migration. From the representative images and the quantitative results (Figure 3A, B), we found that cell viability varied between 80 – 95% during 14 days of culture. There was no significant difference between cell viability in PG2 and Control at incubation times of 3, 7 and 14 days, $p > 0.05$ for all the three time points. Secondly, cell migration in PG2 and Control was studied on Day 3, 7 and 14 post seeding (Figure 3C, D). Cell incorporation and migration is an important characteristic for the scaffold. The depth of cell penetration varied slightly over time (158 – 201 μm) with no significant difference observed between the two scaffolds, $p > 0.05$ for all the three time points. Cell proliferation was evaluated by 5-bromo-2-deoxyuridine (BrdU) assay. As the results (Figure 3E, F) showed, no significant difference was found in the proliferation potential of cells in PG2 (35.2 ± 2.8%) and Control (31.0 ± 1.9%) *in vitro*, $p > 0.05$.

3.3. PG2 enhanced dermis reconstitution in compared with the control dermal substitute.

Under sterile conditions, PG2 and the control scaffold were transplanted into a full-thickness wound mouse model for *in vivo* evaluation. A customized plastic dome with 8 mm diameter, 1.5 mm shoulder and 0.25 mm thickness was applied on the wound bed to prevent skin contraction and to serve as a secure home for scaffolds (Figure 4A) (Marc G Jeschke et al., 2017). There are 24 spaced holes along the edge and six on the top of the dome to ensure air and flow exchange. No macroscopic signs of infection or foreign body reaction were observed in the wound area postoperatively.

Granulation tissue formation is important for skin regeneration and skin healing. The sooner the patients' wounds form granulation tissue, the faster their recovery would be with less mortality and morbidity (Jeschke et al., 2015; Jeschke, Pinto, Costford, & Amini-Nik, 2016). Here in our study granulation tissue formation and maturity were studied by Masson's trichrome staining of the wound sections at day 20 post excisional biopsy and application of scaffolds. Both PG2 and Control showed migration and incorporation of cells within the scaffold (Figure 4B). Besides the newly formed tissue surrounding the scaffold, degradation of the scaffolds was observed, and residues of the scaffold remained in place. High power field (HPF) images (Figure 4C) showed that PG2 on the wound had been degraded into fragments, while the control scaffold remained integrated and undigested. Immature collagen (light blue, thin, and loosely packed) surrounded the fibroblasts on Control treated wound beds, while collagen on PG2 treated wound beds was found mature (bright blue,

dense, and closely packed). Quantification analysis revealed a significantly high degree of granulation tissue formation in PG2 treated wounds (Control: 1.525 ± 0.102 mm^2 per wound; PG2: 2.761 ± 0.386 mm^2 per wound, $p < 0.05$), more mature collagen deposition (Control: 123.79 ± 1.67; PG2: 131.38 ± 2.19 based on the stain intensity, $p < 0.05$) and a higher number of cells (Control: 157.5 ± 7.6 cells per HPF image; PG2: 402.4 ± 22.6 cell per HPF image, $p < 0.001$) in PG2 treated wounds, as compared to Control (Figure 4D - F).

Neovascularization is a critical phenomenon during dermis reconstitution. An ideal scaffold should facilitate angiogenesis (J. Li, Zhang, & Kirsner, 2003; G. Sun et al., 2011). Using immunohistochemical staining for CD31, a marker of endothelial cells, here we showed the size and the density of microvessels on wounds treated with PG2 and Control (Figure S2). While there is a trend of more microvessels in the PG2 scaffold in compare with control, we did not find any significant difference between these two treatments, $p > 0.05$.

Myeloid lineage cells have an essential role during skin healing and dermis reconstitution (Amini-Nik et al., 2014; Bielefeld, Amini-Nik, & Alman, 2013). F4/80 antibody, a macrophage-specific marker, was used to determine the location and the number of macrophages on the wound sites of the two treatments (Figure 5A). To better describe the spatial distribution of macrophages, the wound was divided into the scaffold area and the wound bed (the reconstituted area under the scaffold). Our data showed different spatial patterns of macrophage distribution of these two treatments. In PG2 treated wounds, significantly more macrophages resided in the scaffold area than the wound bed (10.2 ± 1.9% vs. 0.8 ± 0.2%, $p < 0.01$). In contrast, in Control treatment, there were less macrophages resided in the scaffold area in compare with the wound bed area (4.7 ± 1.1% vs. 12.9 ± 3.3%, $p < 0.05$) (Figure 5B). By comparing different treatments, significantly more macrophages were found in PG2 scaffold than Control, $p < 0.05$, while significantly more macrophages on the wound bed of Control than PG2, $p < 0.01$.

While a transient accumulation of myofibroblasts is an essential step during skin healing, their early elimination is accompanying with a less chance of scar formation. To evaluate this on PG2, ASM, a marker of myofibroblast, was used on these histological sections by immunofluorescence staining. There were 33.1 ± 6.6% of ASM positive cells per HPF in Control while there were 8.5 ± 3.2% in PG2 *in vivo* (Figure 6A, B). A significantly low number of ASM positive cells were found on PG2 compared to Control, $p < 0.01$. To further verify this, an *in vitro* experiment of TGF-β1 induced fibroblast to myofibroblast transition was conducted on fibroblasts seeded in PG2 and Control. The ASM expression of cells in different scaffolds was shown in Figure 6C. Consistent with the *in vivo* data, more cells that are positive for ASM expression were observed in Control in compared with PG2 (50.0 ± 4.4% in Control vs. 33.9 ± 3.9% in PG2, $p < 0.05$, Figure 6D).

4. Discussion

Pullulan, as a non-ionic and biodegradable fungal-origin polysaccharide, has been extensively exploited in the food industry due to its non-toxic, non-immunogenic, non-mutagenic and non-carcinogenic nature, but a little effort has been put on the development of its biomedical applications. Thus in this article, we focuses on developing a hybrid

scaffold composed of pullulan and gelatin for skin regeneration. Here, based on our previous data, we report a new generation (the second generation from our lab) of pullulan/gelatin scaffold (PG2) with enhanced physical and chemical properties to scale up for application on the large wounds. The results demonstrated PG2 shows superior biocompatibility in rodents and facilitate dermis reconstitution by comparing with Control, a clinically used dermal regeneration template.

In the preparation of PG2, particulate leaching and crosslinking to pullulan and gelatin were employed to create interior pores and provide stability to the structure. Particulate leaching fabrication technique with salt crystals allowed simple formation of pores and was more environmental-friendly than alternative techniques since the solvent to remove the porogens in the process is water. From the SEM images, we found porous structure within PG2 was successfully generated with this process. Meanwhile, it is known that crosslinking can introduce more chain entanglement and increase stability to the polymer blend, and a dual-crosslinking (crosslinking to pullulan and gelatin respectively) was employed in the fabrication to introduce stability to the final product. The crosslinking mechanism of pullulan by STMP can be explained by a two-step reaction: the ring opening attack of an alcoholate ion on STMP in strong alkaline conditions with the formation of a tripolyphosphated polymer, and the addition of a new polymer chain to form crosslinks (Lack, Dulong, Picton, Cerf, & Condamine, 2007; Mocanu, Mihai, LeCerf, Picton, & Muller, 2004). EDC crosslinker activates carboxyl groups in one gelatin molecule for direct reaction with primary amines of other gelatin molecules via amide bond formation. EDC crosslinking has been proved in improving the strength and stability of collagen-based skin substitutes (Barnes, IV, Brand, Simpson, & Bowlin, 2007; L. Ma, Gao, Mao, Zhou, & Shen, 2004; Powell & Boyce, 2006).

The pore size and the porosity of a scaffold are known to play a significant role in the distribution of nutrients and successful cell encapsulation and migration (Annabi et al., 2010; Loh & Choong, 2013). The range of the pore size of PG2 (20 – 198 μm) is in favor of HDF infiltration (Yannas, Lee, Orgill, Skrabut, & Murphy, 1989). The high porosity and the interconnectivity of PG2 facilitate HDF attachment, migration and proliferation, and also the flow transport of nutrients and metabolic waste products (Chvapil, 1982; Sous et al., 1998). Moreover, water retention capability and the swelling behaviors of PG2 have been determined since it is generally accepted that the ability of dermal substitute to absorb a significant amount of wound exudates whilst maintain a regional moist environment is of critical importance for wound healing and dermis reconstitution (Amini-Nik, Yousuf, & Jeschke, 2018; Mathew N. Nicholas et al., 2016). The swelling profile is another parameter to interpret a porous polymeric scaffold. The fast swelling profile of PG2 is likely attributed to the highly porous structure and the interconnected pores. Moreover, the intrinsic water retention capability of pullulan may contribute into this. While water retention capability is related to a series of physical and chemical factors of materials, such as pore size, porosity and pore wall thickness (Lu et al., 2000; J. Ma, Wang, He, & Chen, 2001; Wei & Ma, 2004), we speculate that the hydrophilicity of the material is another determining factor to water retention, considering that pullulan is a highly hydrophilic polysaccharide. Thus, we believe that pullulan composition in PG2 plays an important role in determining its water uptake and retention. This was supported by our previous reported pullulan-gelatin scaffold, which had

a much higher pullulan composition, exhibited no crosslinking in gelatin, and had higher water retention of 1812 ± 25.46% (Mathew N Nicholas et al., 2016). Even though moisture plays an important role in effective treatment of wounds and it is necessary to keep the wound moist to prevent cell desiccation, it is extremely important to maintain an optimum moist level to prevent bacterial colonization and accelerate healing. Since different wounds have different moisture requirement, no universal standard of moist level of tissue-engineered skin substitute has been established. An ideal dermis scaffold should also match the pace of neo-tissue formation to degrade. While early digestion of scaffold leads to deficient healing and reconstitution, a late degradation of scaffold leads to excessive healing with the possibility of scar formation. This makes biodegradability a necessary feature of skin substitutes. Here PG2 showed a higher degradation (74%) compared to a salt-leached pure gelatin scaffold (45%) reported in the literature (Lee et al., 2005). Although degradation is in direct relation to the crosslinking degree of the scaffolds, here we believe that incorporation of pullulan into the scaffold makes the material more hydrophilic, and allows for easier absorption of liquid and a higher sensitivity to degradation. These results further imply that by manipulating pullulan composition in the scaffold, the degradation can be easily controlled in accordance to different demands.

The degree of cell incorporation into the skin substitute and the ability of cell migration within the materials are of great significance for dermis reconstitution. The microscopic images and the quantification of HDFs incorporated scaffolds provide evidence to support the promising potential of PG2 as a skin substitute, compared to Control. Even though both PG2 and Control show the same depth of cell migration during 14 days *in vitro*, the cells did not migrate significantly over time, likely due to the very low cell seeding density. It is recognized that the seeding density is a major factor affecting cell penetration (Pan et al., 2013). *In vitro* experiments have their own limitation since the interaction with the host body and recruitment of inflammatory cells would be ignored. While *in vitro* the extent of cell migration is comparable, the host may provide microenvironment that facilitates cell migration by degradation of the scaffold. Beside migration, it was worthy noticing here that high viability was maintained over time on both scaffolds despite the very low cell seeding density (around 4000 cells/cm^2) in this study, suggesting that sparse distribution of cells does not affect their viability. As cell number is a determining factor in clinical success, this is critical to clinical applications of PG2 for pre-cellularized dermal substitution approaches since a large number of cells, especially autologous cells, are hard to obtain in an early stage of the treatment, and a low cell seeding density with high viability will be more applicable. Additionally, both scaffolds provided microenvironments for efficient proliferation, an essential property for dermis reconstitution. Overall, *in vitro* evaluation of cell viability, migration and proliferation on both scaffolds demonstrates that PG2 provides a comparable environment to Control for fibroblast infiltration and growth. Despite comparable in the cellular characteristics of PG2 and Control, PG2 is more cost-efficient than Control due to its inexpensive pullulan component.

Based on the *in vitro* data, we hypothesized that the ability of PG2 scaffold to support cell survival and proliferation would facilitate *in vivo* cell migration and neo-tissue formation within the scaffold. To test our hypothesis, an established murine dermis reconstitution model was introduced (Marc G Jeschke et al., 2017).

The presence of the dome on the wound beds prevents contraction, a significant confounding factor that affects the evaluation of skin substitutes (Abdullahi, Amini-Nik, & Jeschke, 2014; Saeid et al., 2011). PG2 on the wound bed provides structural support to cell growth. The plastic domes were effective for securing the scaffold in place and preventing skin contraction while allowing dermis reconstitution.

The significant increase of granulation tissue size, the maturity of collagen and recruited cell numbers on PG2 treated wounds, suggests that wounds treated with PG2 are likely ahead of Control, and PG2 can lead to accelerated healing kinetics. These advantageous phenotypes in granulation tissue formation, cell infiltration and degradation between PG2 and Control led us to investigate the cell types and the mechanism behind the enhanced degradation of PG2 scaffold in the wound area. First, the formation of microvessels was studied considering that angiogenesis and neovascularization are critical determining factors of the wound healing outcomes, especially for deep burn wounds (Jeschke et al., 2015; J. Li et al., 2003; Sadiq et al., 2018). Although no superior on increasing the number and the size of newly formed microvessels was found in PG2 treated wounds, these data still show a signal that PG2 is an ideal home that allows for neovascularization during dermis reconstitution in compare with Control.

To further understand how PG2 promotes healing differently than Control and to determine the distribution of inflammatory cells on PG2, F4/80 staining for macrophages was conducted. Interestingly, these data showed more macrophages in the PG2 scaffold in compare with them in the control scaffold. Considering that we observe less macrophages in the wound bed of PG2 scaffold, these data support the notion that more macrophages recruited from the wound bed into the scaffold in the PG2 treatment. Verifying what triggers this enhanced recruitment is out of the scope of this study at this level but this suggests that efficient inflammatory cell penetration during the dermis reconstitution may accelerate degradation of PG2 scaffold, in addition to hydrolysis. This not only lead to a faster degradation of the scaffold but also provide more free space for mesenchymal cell infiltration and cell proliferation, which may consequently lead to more neo-tissue formation. Altogether, with granulation tissue and cell infiltration data, we suggest that the distinctive structure and composition of PG2 enables optimally paced degradation and promotes the healing process by accelerating disintegration of the scaffold, as compared to Control. As known, macrophages play a significant role during skin healing and hypertrophic scar formation (Amini-Nik et al., 2014; Bielefeld et al., 2013; Saeid et al., 2011). The significantly low macrophages in the reconstituted wound bed area of PG2 are promising in term of scar formation. Further investigation will be needed to verify the beneficial or detrimental effect of this special pattern of macrophage distribution in these skin substitutes. However, a recent study (Hu et al., 2017) provided some insight on the relationship between macrophages transplanted through a pullulan/collagen hydrogel and its therapeutic effect on wound healing. They found similar accelerated healing on macrophage-rich mouse wounds, and proposed a mechanism of a transiently “jump-starting” the inflammatory and neovascular signaling cascades. Despite the different experimental designs between the two studies, we believe that it could be a possible explanation of our observation.

It is known that myofibroblasts contribute to wound closure and scar formation (Amini-Nik, 2018; Amini-Nik et al., 2018; Arno, Amini-Nik, Blit, Al-Shehab, Belo, Herer, & Jeschke, 2014; Bakhtyar et al., 2017; Desmoulière, Chaponnier, & Gabbiani, 2005; Mak et al., 2009; Moulin, Auger, Garrel, & Germain, 2000). Therefore, sustained myofibroblast presence in the proliferation phase of wound healing, while important in the early phase, can lead to scar formation. Presence of myofibroblasts on both scaffolds was studied with these histological sections. The result of fewer myofibroblasts in PG2 implies that, compared to Control, PG2 either decreased the extent of fibroblast to myofibroblast differentiation or due to the rapid degradation of the scaffold the transient myofibroblastic phase was passed. To verify this, the *in vitro* experiment of TGF-β1 induced fibroblast to myofibroblast differentiation was conducted on the fibroblasts in PG2 and Control. In agreement with the observation *in vivo*, fewer myofibroblasts were observed on PG2. This further supports that cells in PG2 are less myofibroblastic compared to Control and PG2 treatment may provide a positive effect on attenuating scar formation attributed to its own material properties. Since mice cannot develop scars during skin healing and skin regeneration, further experiments in larger animals such as pigs and horses are necessary to unravel the anti-scar properties of PG2. While *in vivo* rodent experiments are more feasible in term of the cost and the number of biological replicates that we can use, it is associated with several limitations. The contractile property of rodents' skin dominates the healing process as they mainly heal with contraction. Our model eliminates this confounding factor by inhibiting the contraction and specifically evaluates the extent of dermis reconstitution. While advantageous, it would be difficult to comment on the wound size as that size has been kept constant with a dome. It is also difficult to evaluate the extent of re-epithelialization. As such this model has been used to merely address dermis reconstitution and we compared PG2 with a commercial dermal substitute. Whether PG2 can facilitate re-epithelialization is out of the scope of this project and needs modified dome models or lager animal models. However, it is shown that faster granulation tissue formation strengthens re-epithelialization (Bielefeld et al., 2013). As such, in larger wounds, we speculate that PG2 indirectly augments re-epithelialization by enhancing granulation tissue formation. Nevertheless, we only reported on the dermal component of reconstituted skin and demonstrated that PG2 enhance dermal reconstitution.

5. Conclusion

In this study, a PG2 dermal substitute was prepared using a particulate leaching/crosslinking fabrication technique which showed excellent potential as a dermal skin substitute. *In vitro*, PG2 is biocompatible with the main cellular component of dermis: fibroblasts. Grafting of PG2 onto the mice with full thickness skin wounds led to a high degree of granulation tissue formation, more matured collagen, and more cell presence on the wounds, followed by a faster disintegration of PG2 scaffold. The faster degradation of PG2 was associated with the higher number of macrophages in the scaffold, suggesting its contribution to a higher degree of scaffold degradation compared to the commercial control. A lower number of α-smooth muscle actin positive cells in PG2 demonstrated fewer myofibroblasts in PG2 treated wounds and suggested a potential for attenuating scar formation during wound healing.

Supplementary Material

Refer to Web version on PubMed Central for supplementary material.

Acknowledgements

The authors would like to thank our funding sources: Toronto Hydro (Donation), Canadian Institutes of Health Research (MGJ: No. 123336), National Institutes of Health (MGJ and SAN: NIH RO1 GM087285–01), Medicine by Design (SAN and MGJ: EMH SEED grant) and Ontario Institute for Regenerative Medicine (MGJ and SAN: 7/2018). We would like to thank Dr. Kirsten Bielefeld (Sunnybrook Research Institute) for proofreading and review of the manuscript.

References

Abdullahi A, Amini-Nik S, & Jeschke MG (2014). Animal models in burn research. Cellular and molecular life sciences : CMLS, 71(17), 3241–3255. doi:10.1007/s00018-014-1612-5 [PubMed: 24714880]

Aljghami ME, Jeschke MG, & Amini-Nik S (2019). Examining the contribution of surrounding intact skin during cutaneous healing. J Anat, 234(4), 523–531. doi:10.1111/joa.12941 [PubMed: 30786015]

Aljghami ME, Saboor S, & Amini-Nik S (2019). Emerging Innovative Wound Dressings. Ann Biomed Eng, 47(3), 659–675. doi:10.1007/s10439-018-02186-w [PubMed: 30542783]

Amini-Nik S (2018). Time Heals all Wounds- but Scars Remain. Can Personalized Medicine Help? Frontiers in genetics, 9, 211–211. doi:10.3389/fgene.2018.00211 [PubMed: 29988374]

Amini-Nik S, Cambridge E, Yu W, Guo A, Whetstone H, Nadesan P, . . . Alman BA (2014). β-Catenin–regulated myeloid cell adhesion and migration determine wound healing. The Journal of Clinical Investigation, 124(6), 2599–2610. doi:10.1172/JCI62059 [PubMed: 24837430]

Amini-Nik S, Yousuf Y, & Jeschke MG (2018). Scar management in burn injuries using drug delivery and molecular signaling: Current treatments and future directions. Advanced Drug Delivery Reviews, 123, 135–154. doi:10.1016/j.addr.2017.07.017 [PubMed: 28757325]

Annabi N, Nichol JW, Zhong X, Ji C, Koshy S, Khademhosseini A, & Dehghani F (2010). Controlling the Porosity and Microarchitecture of Hydrogels for Tissue Engineering. Tissue Engineering Part B: Reviews, 16(4), 371–383. doi:10.1089/ten.teb.2009.0639 [PubMed: 20121414]

Arno AI, Amini-Nik S, Blit PH, Al-Shehab M, Belo C, Herer E, & Jeschke MG (2014). Effect of human Wharton's jelly mesenchymal stem cell paracrine signaling on keloid fibroblasts. Stem cells translational medicine, 3(3), 299–307. doi:10.5966/sctm.2013-0120 [PubMed: 24436441]

Arno AI, Amini-Nik S, Blit PH, Al-Shehab M, Belo C, Herer E, . . . Jeschke MG (2014). Human Wharton's jelly mesenchymal stem cells promote skin wound healing through paracrine signaling. Stem Cell Research & Therapy, 5(1), 28. doi:10.1186/scrt417 [PubMed: 24564987]

Bakhtyar N, Jeschke MG, Mainville L, Herer E, & Amini-Nik S (2017). Acellular Gelatinous Material of Human Umbilical Cord Enhances Wound Healing: A Candidate Remedy for Deficient Wound Healing. Frontiers in physiology, 8, 200–200. doi:10.3389/fphys.2017.00200 [PubMed: 28421003]

Barnes CP IV, P. CW, Brand DD, Simpson DG, & Bowlin GL (2007). Cross-Linking Electrospun Type II Collagen Tissue Engineering Scaffolds with Carbodiimide in Ethanol. Tissue Engineering, 13(7), 1593–1605. doi:10.1089/ten.2006.0292 [PubMed: 17523878]

Bielefeld KA, Amini-Nik S, & Alman BA (2013). Cutaneous wound healing: recruiting developmental pathways for regeneration. Cellular and Molecular Life Sciences, 70(12), 2059–2081. doi:10.1007/s00018-012-1152-9 [PubMed: 23052205]

Branski LK, Herndon DN, Pereira C, Mlcak RP, Celis MM, Lee JO, . . . Jeschke MG (2007). Longitudinal assessment of Integra in primary burn management: a randomized pediatric clinical trial. Critical care medicine, 35(11), 2615–2623. [PubMed: 17828040]

Chvapil M (1982). Considerations on manufacturing principles of a synthetic burn dressing: a review. Journal of Biomedical Materials Research Part A, 16(3), 245–263.

Desmoulière A, Chaponnier C, & Gabbiani G (2005). Tissue repair, contraction, and the myofibroblast. Wound repair and regeneration, 13(1), 7–12. [PubMed: 15659031]

Hu MS, Walmsley GG, Barnes LA, Weiskopf K, Rennert RC, Duscher D, . . . Longaker MT (2017). Delivery of monocyte lineage cells in a biomimetic scaffold enhances tissue repair. JCI insight, 2(19), e96260. doi:10.1172/jci.insight.96260

Jeschke MG, Patsouris D, Stanojcic M, Abdullahi A, Rehou S, Pinto R, . . . Amini-Nik S (2015). Pathophysiologic Response to Burns in the Elderly. EBioMedicine, 2(10), 1536–1548. doi:10.1016/j.ebiom.2015.07.040 [PubMed: 26629550]

Jeschke MG, Pinto R, Costford SR, & Amini-Nik S (2016). Threshold age and burn size associated with poor outcomes in the elderly after burn injury. Burns, 42(2), 276–281. doi:10.1016/j.burns.2015.12.008 [PubMed: 26803373]

Jeschke MG, Sadri A-R, Belo C, & Amini-Nik S (2017). A surgical device to study the efficacy of bioengineered skin substitutes in mice wound healing models. Tissue Engineering Part C: Methods, 23(4), 237–242. [PubMed: 28338428]

Jeschke MG, Sadri AR, Belo C, & Amini-Nik S (2017). A Surgical Device to Study the Efficacy of Bioengineered Skin Substitutes in Mice Wound Healing Models. Tissue Eng Part C Methods, 23(4), 237–242. doi:10.1089/ten.tec.2016.0545 [PubMed: 28338428]

Lack S, Dulong V, Picton L, Cerf DL, & Condamine E (2007). High-resolution nuclear magnetic resonance spectroscopy studies of polysaccharides crosslinked by sodium trimetaphosphate: a proposal for the reaction mechanism. Carbohydrate Research, 342(7), 943–953. doi:10.1016/j.carres.2007.01.011 [PubMed: 17303095]

Leathers TD (2003). Biotechnological production and applications of pullulan. Applied Microbiology and Biotechnology, 62(5), 468–473. doi:10.1007/s00253-003-1386-4 [PubMed: 12830329]

Lee SB, Kim YH, Chong MS, Hong SH, & Lee YM (2005). Study of gelatin-containing artificial skin V: fabrication of gelatin scaffolds using a salt-leaching method. Biomaterials, 26(14), 1961–1968. doi:10.1016/j.biomaterials.2004.06.032 [PubMed: 15576170]

Li J, Zhang YP, & Kirsner RS (2003). Angiogenesis in wound repair: angiogenic growth factors and the extracellular matrix. Microscopy research and technique, 60(1), 107–114. [PubMed: 12500267]

Li X, Xue W, Liu Y, Fan D, Zhu C, & Ma X (2015). Novel multifunctional PB and PBH hydrogels as soft filler for tissue engineering. Journal of Materials Chemistry B, 3(23), 4742–4755.

Loh QL, & Choong C (2013). Three-Dimensional Scaffolds for Tissue Engineering Applications: Role of Porosity and Pore Size. Tissue Engineering Part B: Reviews, 19(6), 485–502. doi:10.1089/ten.teb.2012.0437

Lu L, Peter SJ, Lyman MD, Lai H-L, Leite SMA, Tamada J, . . . Mikos AG (2000). In vitro degradation of porous poly(l-lactic acid) foams. Biomaterials, 21(15), 1595–1605. doi:10.1016/S0142-9612(00)00048-X [PubMed: 10885732]

Ma J, Wang H, He B, & Chen J (2001). A preliminary in vitro study on the fabrication and tissue engineering applications of a novel chitosan bilayer material as a scaffold of human neofetal dermal fibroblasts. Biomaterials, 22(4), 331–336. doi:10.1016/S0142-9612(00)00188-5 [PubMed: 11205436]

Ma L, Gao C, Mao Z, Zhou J, & Shen J (2004). Enhanced biological stability of collagen porous scaffolds by using amino acids as novel cross-linking bridges. Biomaterials, 25(15), 2997–3004. doi:10.1016/j.biomaterials.2003.09.092 [PubMed: 14967532]

Mak K, Manji A, Gallant-Behm C, Wiebe C, Hart DA, Larjava H, & Häkkinen L (2009). Scarless healing of oral mucosa is characterized by faster resolution of inflammation and control of myofibroblast action compared to skin wounds in the red Duroc pig model. Journal of Dermatological Science, 56(3), 168–180. doi:10.1016/j.jdermsci.2009.09.005 [PubMed: 19854029]

Mano JF, Silva GA, Azevedo HS, Malafaya PB, Sousa RA, Silva SS, . . . Reis RL (2007). Natural origin biodegradable systems in tissue engineering and regenerative medicine: present status and some moving trends. Journal of The Royal Society Interface, 4(17), 999.

Mocanu G, Mihai D, LeCerf D, Picton L, & Muller G (2004). Synthesis of new associative gel microspheres from carboxymethyl pullulan and their interactions with lysozyme. European Polymer Journal, 40(2), 283–289. doi:10.1016/j.eurpolymj.2003.09.019

Moiemen N, Yarrow J, Hodgson E, Constantinides J, Chipp E, Oakley H, . . . Freeth M (2011). Long-Term Clinical and Histological Analysis of Integra Dermal Regeneration Template. Plastic and Reconstructive Surgery, 127(3), 1149–1154. doi:10.1097/PRS.0b013e31820436e3 [PubMed: 21088647]

Moiemen NS, Staiano JJ, Ojeh NO, Thway Y, & Frame JD (2001). Reconstructive surgery with a dermal regeneration template: clinical and histologic study. Plastic and reconstructive surgery, 108(1), 93–103. doi:10.1097/00006534-200107000-00015 [PubMed: 11420509]

Moulin V, Auger FA, Garrel D, & Germain L (2000). Role of wound healing myofibroblasts on re-epithelialization of human skin. Burns, 26(1), 3–12. doi:10.1016/S0305-4179(99)00091-1 [PubMed: 10630313]

Nicholas MN, Jeschke MG, & Amini-Nik S (2016). Cellularized Bilayer Pullulan-Gelatin Hydrogel for Skin Regeneration. Tissue Engineering Part A, 22(9–10), 754–764. [PubMed: 27072720]

Nicholas MN, Jeschke MG, & Amini-Nik S (2016). Methodologies in creating skin substitutes. Cellular and molecular life sciences : CMLS, 73(18), 3453–3472. doi:10.1007/s00018-016-2252-8 [PubMed: 27154041]

Pan Z, Ghosh K, Hung V, Macri LK, Einhorn J, Bhatnagar D, . . . Rafailovich MH (2013). Deformation gradients imprint the direction and speed of en masse fibroblast migration for fast healing. Journal of Investigative Dermatology, 133(10), 2471–2479. [PubMed: 23594599]

Powell HM, & Boyce ST (2006). EDC cross-linking improves skin substitute strength and stability. Biomaterials, 27(34), 5821–5827. doi:10.1016/j.biomaterials.2006.07.030 [PubMed: 16919327]

Rnjak J, Wise SG, Mithieux SM, & Weiss AS (2010). Severe Burn Injuries and the Role of Elastin in the Design of Dermal Substitutes. Tissue Engineering Part B: Reviews, 17(2), 81–91. doi:10.1089/ten.teb.2010.0452

Rustad KC, Wong VW, Sorkin M, Glotzbach JP, Major MR, Rajadas J, . . . Gurtner GC (2012). Enhancement of mesenchymal stem cell angiogenic capacity and stemness by a biomimetic hydrogel scaffold. Biomaterials, 33(1), 80–90. doi:10.1016/j.biomaterials.2011.09.041 [PubMed: 21963148]

Sadiq A, Shah A, Jeschke GM, Belo C, Qasim Hayat M, Murad S, & Amini-Nik S (2018). The Role of Serotonin during Skin Healing in Post-Thermal Injury. International Journal of Molecular Sciences, 19(4). doi:10.3390/ijms19041034

Saeid AN, Dylan G, Corey B, Heather W, Charles K, & A. AB (2011). Pax7 Expressing Cells Contribute to Dermal Wound Repair, Regulating Scar Size through a β-Catenin Mediated Process. STEM CELLS, 29(9), 1371–1379. doi:doi:10.1002/stem.688 [PubMed: 21739529]

Sheikholeslam M, Wright MEE, Jeschke MG, & Amini-Nik S (2017). Biomaterials for Skin Substitutes. Advanced Healthcare Materials, 7(5), 1700897. doi:10.1002/adhm.201700897

Soller EC, Tzeranis DS, Miu K, So PTC, & Yannas IV (2012). Common features of optimal collagen scaffolds that disrupt wound contraction and enhance regeneration both in peripheral nerves and in skin. Biomaterials, 33(19), 4783–4791. doi:10.1016/j.biomaterials.2012.03.068 [PubMed: 22483241]

Sous M, Bareille R, Rouais F, Clement D, Amedee J, Dupuy B, & Baquey C (1998). Cellular biocompatibility and resistance to compression of macroporous β-tricalcium phosphate ceramics. Biomaterials, 19(23), 2147–2153. [PubMed: 9884055]

Sun BK, Siprashvili Z, & Khavari PA (2014). Advances in skin grafting and treatment of cutaneous wounds. Science, 346(6212), 941–945. doi:10.1126/science.1253836 [PubMed: 25414301]

Sun G, Zhang X, Shen Y-I, Sebastian R, Dickinson LE, Fox-Talbot K, . . . Gerecht S (2011). Dextran hydrogel scaffolds enhance angiogenic responses and promote complete skin regeneration during burn wound healing. Proceedings of the National Academy of Sciences, 108(52), 20976.

Wang H-M, Chou Y-T, Wen Z-H, Wang Z-R, Chen C-H, & Ho M-L (2013). Novel Biodegradable Porous Scaffold Applied to Skin Regeneration. PLOS ONE, 8(6), e56330. doi:10.1371/journal.pone.0056330 [PubMed: 23762223]

Wang T-W, Sun J-S, Wu H-C, Tsuang Y-H, Wang W-H, & Lin F-H (2006). The effect of gelatin–chondroitin sulfate–hyaluronic acid skin substitute on wound healing in SCID mice. Biomaterials, 27(33), 5689–5697. doi:10.1016/j.biomaterials.2006.07.024 [PubMed: 16908060]

Wei G, & Ma PX (2004). Structure and properties of nano-hydroxyapatite/polymer composite scaffolds for bone tissue engineering. Biomaterials, 25(19), 4749–4757. doi:10.1016/j.biomaterials.2003.12.005 [PubMed: 15120521]

Wong VW, Rustad KC, Glotzbach JP, Sorkin M, Inayathullah M, Major MR, . . . Gurtner GC (2011). Pullulan Hydrogels Improve Mesenchymal Stem Cell Delivery into High-Oxidative-Stress Wounds. Macromolecular bioscience, 11(11), 1458–1466. doi:10.1002/mabi.201100180 [PubMed: 21994074]

Xiong S, Zhang X, Lu P, Wu Y, Wang Q, Sun H, . . . Ouyang H (2017). A Gelatin-sulfonated Silk Composite Scaffold based on 3D Printing Technology Enhances Skin Regeneration by Stimulating Epidermal Growth and Dermal Neovascularization. Scientific Reports, 7(1), 4288. doi:10.1038/s41598-017-04149-y [PubMed: 28655891]

Yannas I, Lee E, Orgill DP, Skrabut E, & Murphy GF (1989). Synthesis and characterization of a model extracellular matrix that induces partial regeneration of adult mammalian skin. Proceedings of the National Academy of Sciences, 86(3), 933–937.

Zhao X, Lang Q, Yildirimer L, Lin ZY, Cui W, Annabi N, . . . Khademhosseini A (2016). Photocrosslinkable Gelatin Hydrogel for Epidermal Tissue Engineering. Advanced Healthcare Materials, 5(1), 108–118. doi:10.1002/adhm.201500005 [PubMed: 25880725]

Zhao X, Sun X, Yildirimer L, Lang Q, Lin ZY, Zheng R, . . . Khademhosseini A (2017). Cell infiltrative hydrogel fibrous scaffolds for accelerated wound healing. Acta Biomaterialia, 49, 66–77. doi:10.1016/j.actbio.2016.11.017 [PubMed: 27826004]

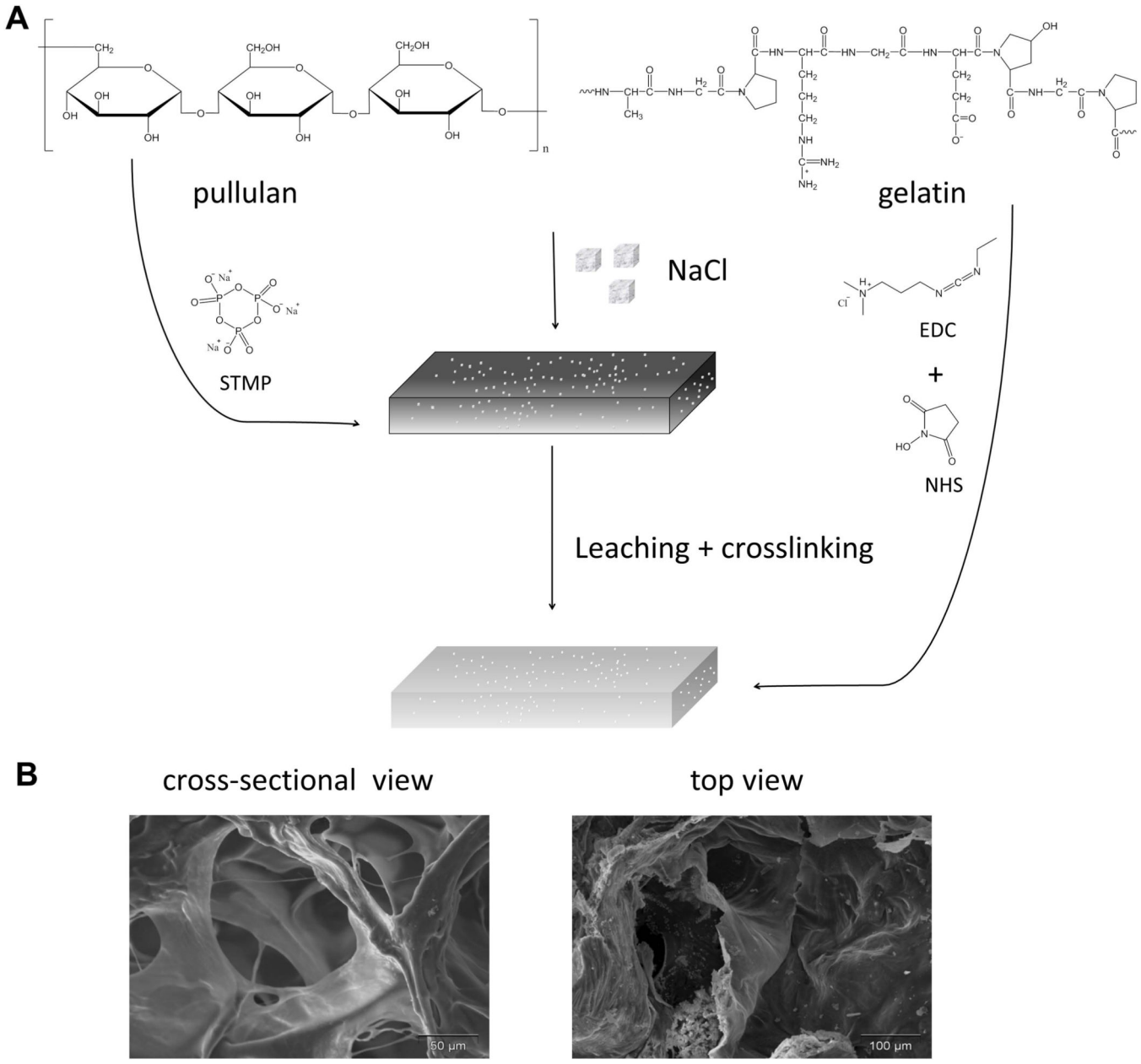

Figure 1.

Preparation of PG2 by a combined particulate leaching/crosslinking process (A); the morphology of PG2 by scanning electronic microscopy (SEM) (B).

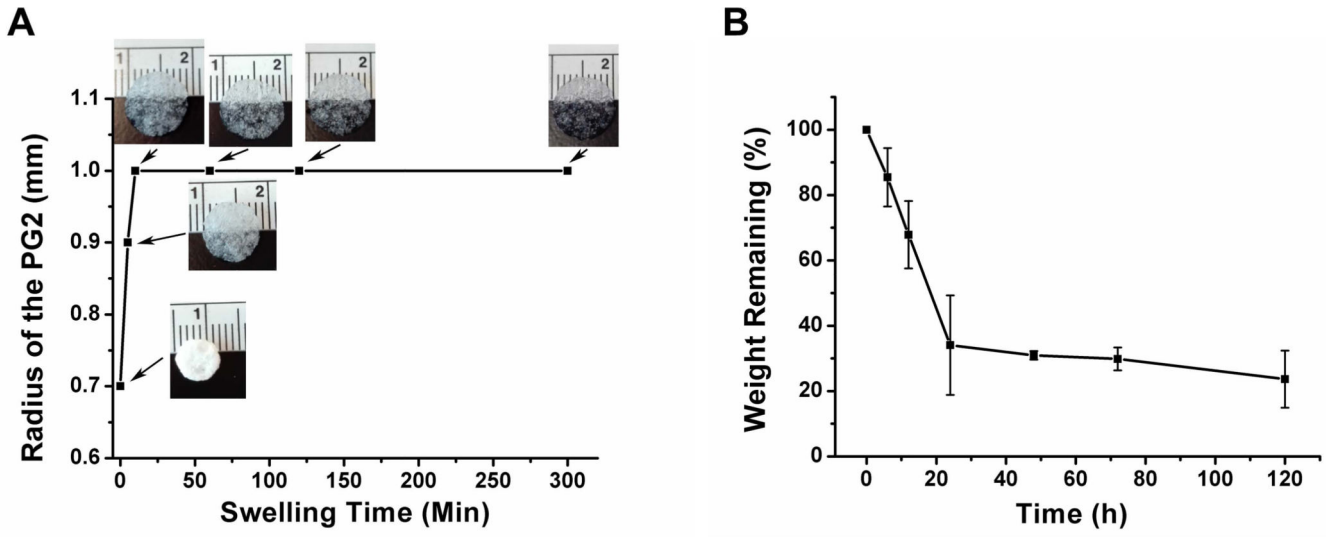

Figure 2.

Swelling profile of PG2 with representative images (A); enzyme degradation profile of PG2 in collagenase I PBS solution (B).

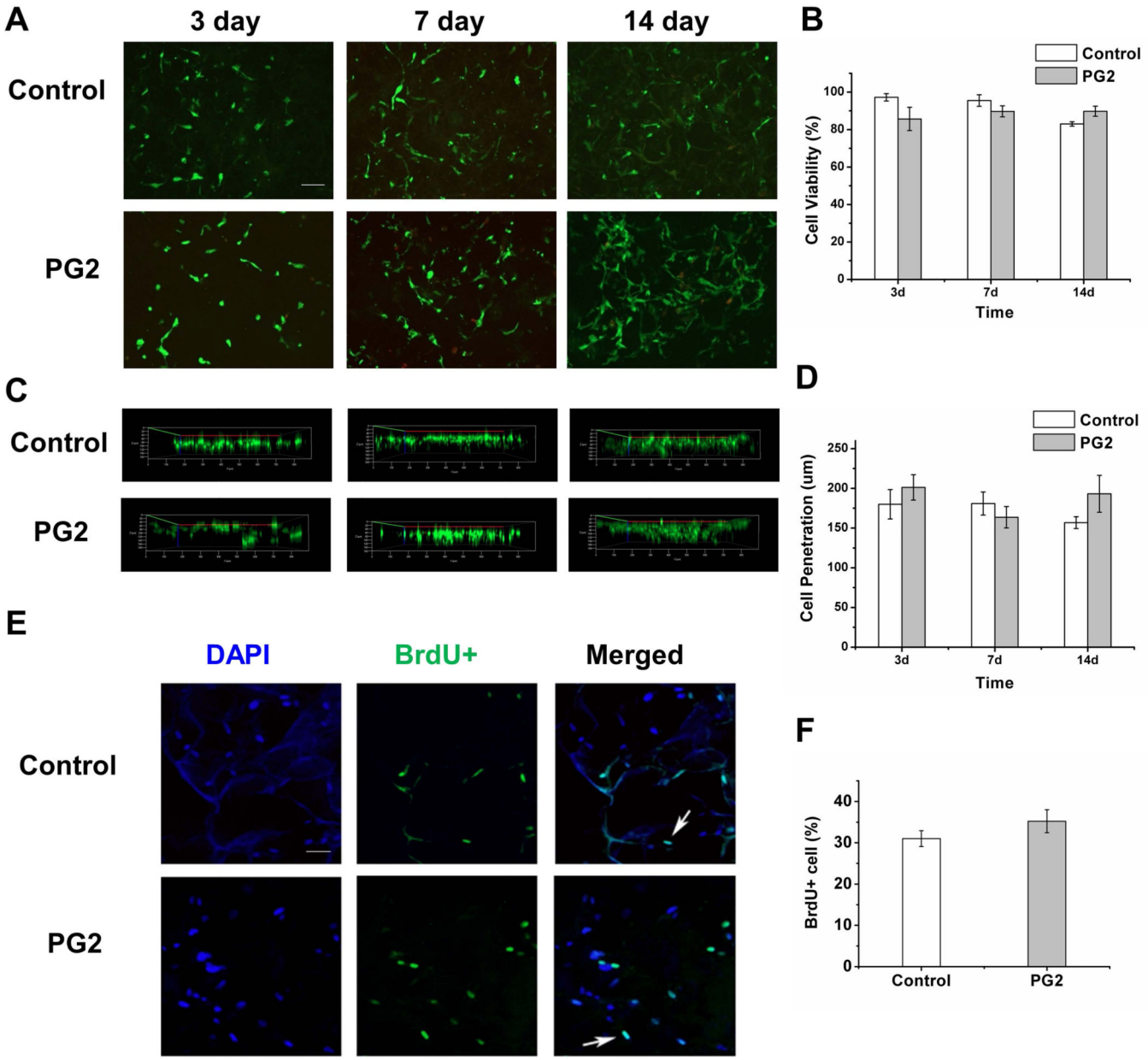

Figure 3.

PG2 is biocompatible *in vitro*. Representative images of HDFs in PG2 and Control at 3, 7 and 14 days of culture, stained by Live/Dead assay (*Green*: live cells labeled by calcein AM; *red*: dead cells labeled by ethidium homodimer-1) (A), scale bar = 100 μm, quantified in B; representative 3D reconstruction of the Z-stack images showing the extent of cell migration in PG2 and Control at 3, 7 and 14 days (C), quantified in D; representative images of HDFs in PG2 and Control showing the extent of BrdU incorporation using BrdU assay (*Blue*: DAPI; *green*: BrdU) (E), scale bar = 50 μm, quantified in F.

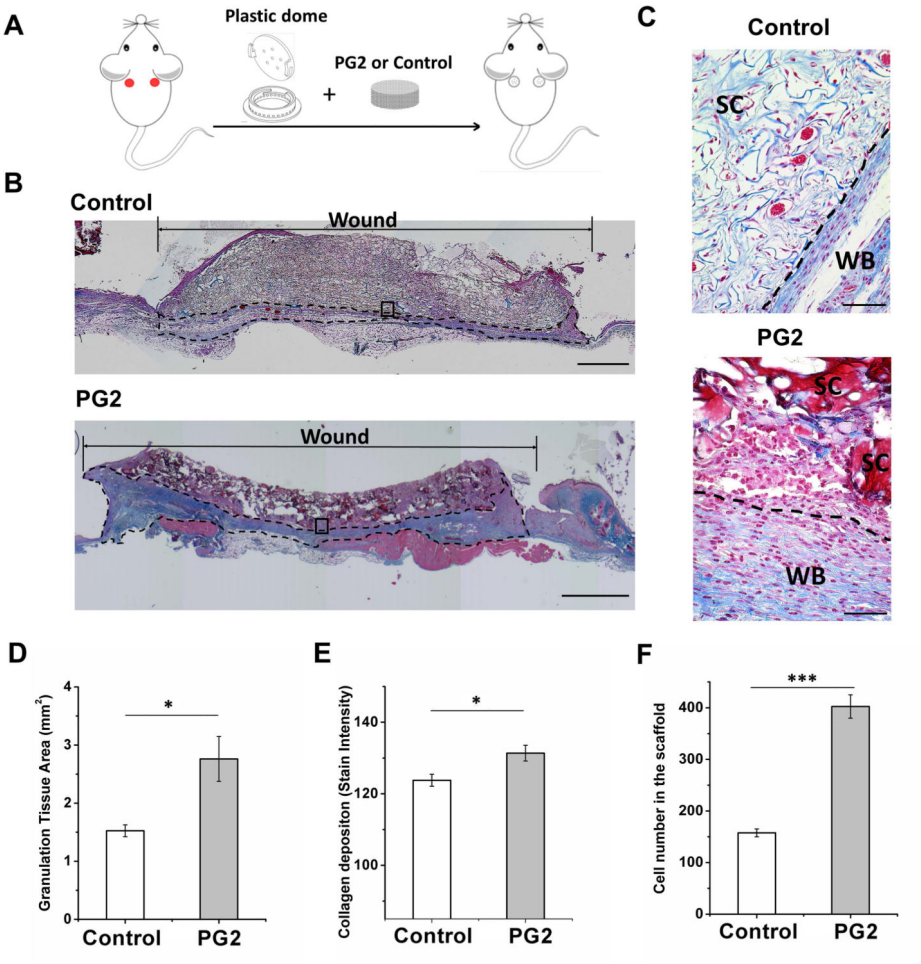

Figure 4.

PG2 enhance grannnulation tissue formation with higher cellularity and more collagen deposition. Scheme of the mouse model (A); representative Masson's trichrome stained images to show a complete view of wounds treated with PG2 and Control by day 20, the dotted line marks collagen formation (B), scale bar = 1 mm; histological sections at 40X magnification showed scaffold fragments of PG2 and an integrated layer of Control (C), scale bar = 50 μm, SC, the scaffold or the scaffold fragment; WB, wound bed and collagen fiber deposition; quantification of granulation tissue area (D), collagen depositon (E) and infiltrated cell number (F) to demonstrate rapid, efficient and functional formation of neo-tissue. *$p < 0.05$, **$p < 0.01$, ***$p < 0.001$.

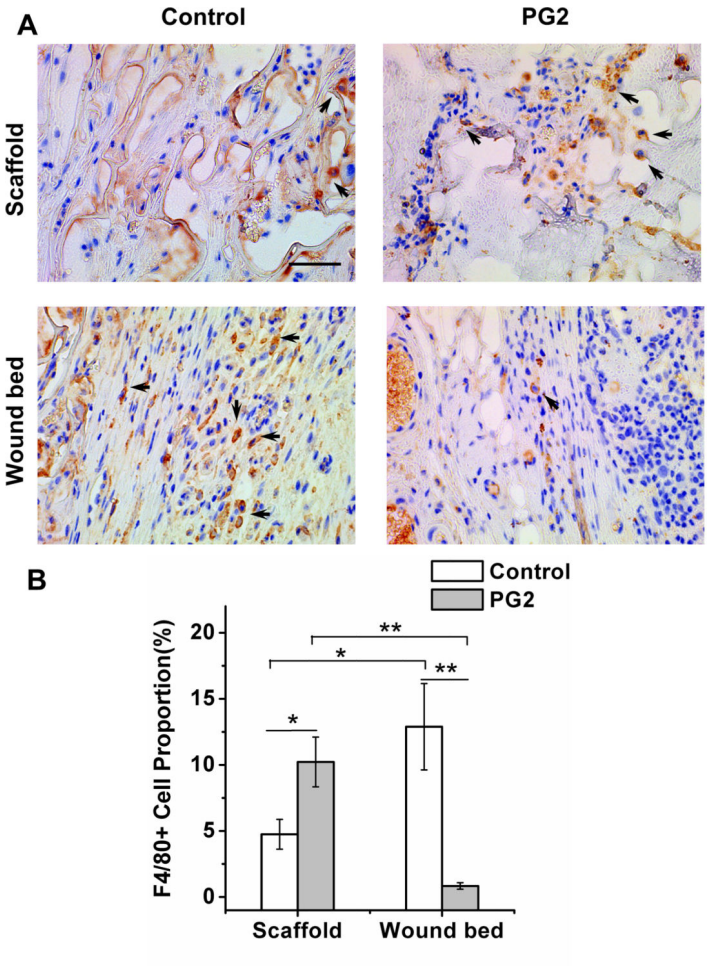

Figure 5.

Unlike the scaffold area, wound bed of the PG2 sccafold has less number of F4/80+ve macrophages. Histological sections of wounds treated with PG2 and Control on day 20, stained with F4/80 (macrophages as arrows indicated) (A), scale bar = 50 μm; quantification of F4/80+ve cell (macrophage) proportion on wounds with different treatments at two different locations (B).

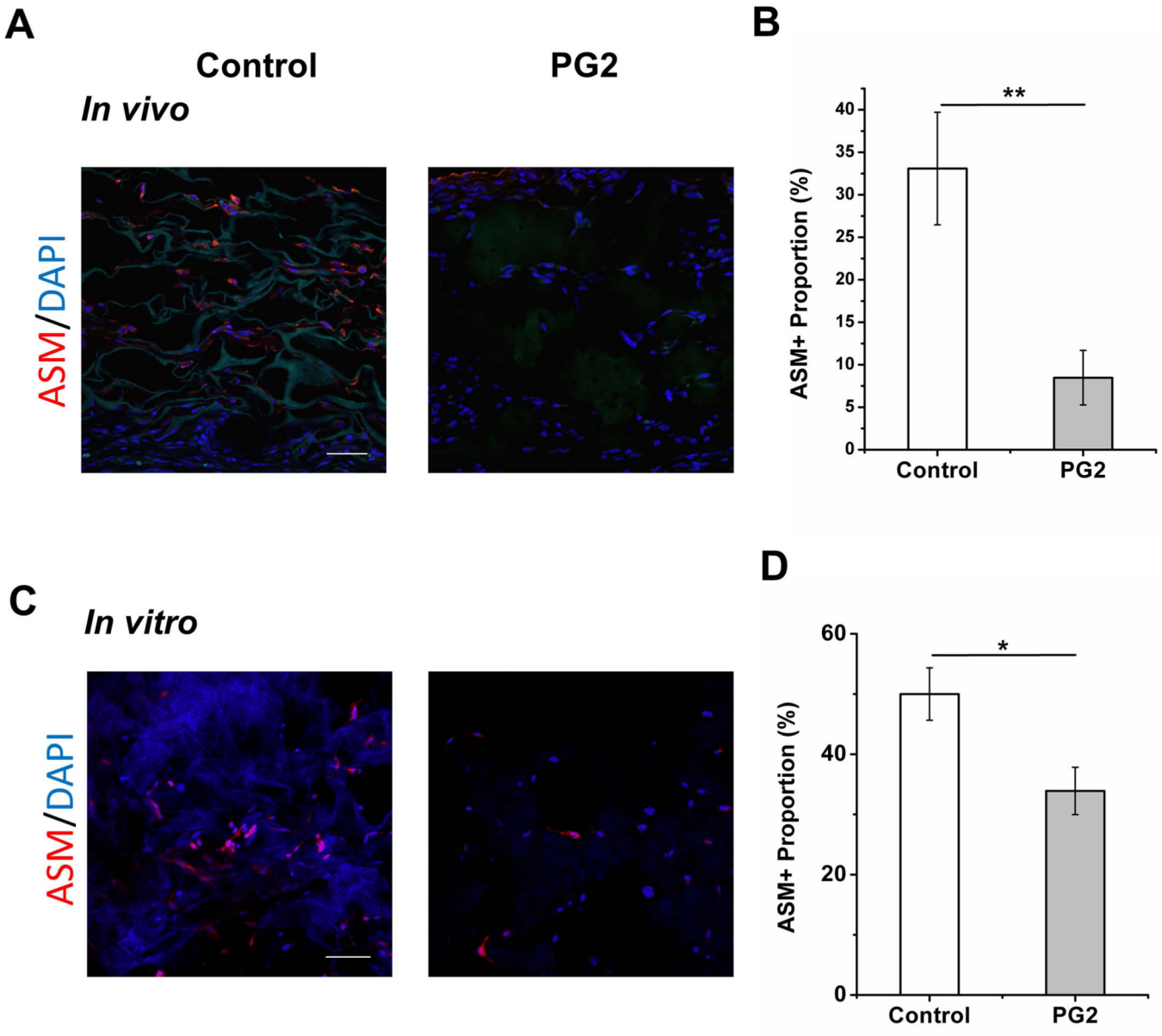

Figure 6.

The PG2 scaffold enhances less myofibroblastic phenotype. Immunofluorescent sections of wounds dressed with PG2 and Control on day 20 (A) and HDFs cultured in PG2 and Control *in vitro* 48h after TGF-β1 induction, stained with ASM (myofibroblast), to demonstrate myofibroblast differentiation in different scaffolds(C), scale bar = 100 μm; quantification results of ASM+ve cell proportion on wounds with different treatments *in vivo* (B) and in different scaffolds *in vitro* (D).